CHAPTER ELEVEN

# Microelectrophoretic single-cell measurements with microfluidic devices

**Jay Sibbitts, Jalal Sadeghi, Christopher T. Culbertson***
Department of Chemistry, Kansas State University, Manhattan, KS, United States
*Corresponding Author: e-mail address: culbert@ksu.edu

## Contents

1. Introduction 224
2. Importance and analysis of intracellular NO 225
3. Device overview 226
   3.1 Device design and working principles 226
   3.2 Improvements in optical fiber detection 228
4. Materials and methods 229
   4.1 Reagents and materials 229
   4.2 Device fabrication 230
   4.3 Experimental setup 234
   4.4 Cell culture and preparation 236
5. Notes 238
6. Conclusion 239
Acknowledgments 239
References 240

## Abstract

Here we describe in detail the design, fabrication and operation of our automated high-throughput single cell microchip electrophoresis device with laser induced fluorescence detection. Our device features on-board integrated peristaltic pumps that generate flow directly within the microfluidic channels. Additionally, we have incorporated an optical fiber bridge that enables simultaneous fluorescence detection at two points of interest within the device without the need for additional optical components or detectors. The second detection spot is used to detect the intact cell immediately prior to lysis giving a signal at $t = 0$ s for each single-cell electropherogram. We can also use this signal to measure the absolute migration time of the separated analytes to confidently determine the identity of each peak. Finally, we demonstrate the application of our device for the measurement of intracellular nitric oxide (NO) levels in T-lymphocytes. Changes in NO levels within cells is associated with a number of chronic diseases including neurodegenerative, cardiovascular and cancers. We show that our

*Methods in Enzymology*, Volume 628
ISSN 0076-6879
https://doi.org/10.1016/bs.mie.2019.07.011

system is capable of measuring NO levels under the following conditions: native, lipopolysaccharide stimulation, and inhibition of inducible nitric oxide synthase. It is our hope that the information and procedures described in this chapter may enable others to use or adapt our system for other analyses at the single cell level.

## 1. Introduction

Integrated microfluidic devices have become very versatile tools for biological and biomedical investigations (Patabadige, Jia, et al., 2016; Sibbitts, Sellens, Jia, Klasner, & Culbertson, 2018). Devices capable of single-cell analysis (SCA), in particular, have proven useful in the study of the etiology of several chronic illnesses including cardiovascular disease (Bektik, Dennis, Prasanna, Madabhushi, & Fu, 2017), neurodegenerative diseases (Metto et al., 2013), and cancers (Turner et al., 2016). The SCA devices presented in these studies address key challenges in the analysis of diseases, such as heterogeneity within the affected cell populations and the tendency of enzyme activities to change on relatively short time scales.

Microchip electrophoresis coupled with laser induced fluorescence detection (μCE-LIF) is among the more powerful modes of SCA due to the combination of automated cell handling enabled by microfluidics, the speed of electrophoretic separations, and the sensitivity of LIF detection. There are several current analysis methods that use fluorescent probes to measure the activity of enzymes such as kinases (Dickinson et al., 2015; Proctor et al., 2014) proteases (Wang et al., 2016), nitric oxide synthases, and oxidases (Caruso, Fresta, Siegel, Wijesinghe, & Lunte, 2017; Chen et al., 2012; Mainz et al., 2012; Metto et al., 2013). Some of these probes directly measure enzyme activity using fluorescently labeled peptide probes while other measure the products of enzyme activity (i.e., nitric oxide and superoxide) using reactive fluorescent moieties. These methodologies are readily adaptable to μCE-LIF device.

For several years our research group has been developing automated high-throughput single cell μCE-LIF devices. We have made concerted efforts to improve the robustness and ease-of-use of our devices, and therefore, the goal of this chapter is to provide detailed and comprehensive methods for the fabrication and operation of our previously published integrated fiber optic single-cell analysis system (Patabadige, Jia, et al., 2016; Sadeghi, Patabadige, Culbertson, Latifi, & Culbertson, 2016) and

to demonstrate how it may be used to measure inducible nitric oxide synthase (iNOS) activity in T-lymphocytes through the quantitation of intracellular nitric oxide (NO) under native, stimulated, and inhibited conditions.

## 2. Importance and analysis of intracellular NO

Nitric oxide (NO) is a fundamental intercellular signaling molecule that is associated with the control and regulation of many major cellular functions including immune response (Bogdan, 2001), anti-inflammatory response (Pacher, Beckman, & Liaudet, 2007), and neurotransmission (Pacher et al., 2007). Increased levels of NO can lead to nitrosative stress states in cells that can cause damage to DNA or disrupt certain enzymatic activities (Caruso et al., 2017). The effects of nitrosative stress have been linked to several chronic illnesses including neurodegenerative and cardiovascular diseases as well as a number of different cancers (Pacher et al., 2007). NO exists in vivo as a dissolved free radical gas, with an unpaired electron on the nitrogen. It is produced in cells by a family of nitric oxide synthase enzymes (NOS): endothelial nitric oxide synthase (eNOS), neuronal nitric oxide synthase (nNOS), and induced nitric oxide synthase (iNOS). Upon reaction with the superoxide anion ($O_2^{\cdot-}$), NO forms the highly reactive species peroxynitrite ($ONOO^-$). Peroxynitrite can cause substantial damage to biological systems through nitration, nitrosylation, and the oxidation of proteins, DNA, and lipids. The ability to monitor the production of NO may aid in the understanding of its role in the progression of these diseases. However, NO has a relatively short half-life (3–6 s) (Pacher et al., 2007), and therefore analysis must be performed rapidly to obtain accurate measurements. Rapid measurement of intracellular NO may be achieved using DAF-FM DA (4-amino-5-methylamino-2′,7′-difluorofluorescein diacetate). DAF-FM DA is a non-fluorescent, membrane permeant molecule that may passively diffuse across cell membranes. Upon entry into the cell, it is deacylated by intracellular esterases, forming a membrane impermeant species, DAF-FM. It then reacts with nitric oxide to form a highly fluorescent benzotriazole derivative reporter, DAF-FM T. To account for differences in loading efficiency and esterase activity, an internal standard 6-carboxyfluorescein diacetate (6-CFDA) can be added, as it is structurally similar to DAF-FM DA and is also deacylated by esterase enzymes to form 6-carboxyfluorescein (6-CF) within the cells (Metto et al., 2013).

# 3. Device overview

## 3.1 Device design and working principles

The working principles and operation of the microfluidic device, integrated soft lithographic pumps, and integrated optical fiber detection were described in depth previously (Patabadige, Mickleburgh, et al., 2016; Patabadige, Sadeghi, et al., 2016). Briefly, labeled cells are loaded into the sample reservoir (labeled "S" in Fig. 1A) and drawn to the lysis intersection via hydrodynamic flow generated by the on-board peristaltic pumps (Fig. 1A). Fluorophores within the intact cells are excited as they pass underneath the cell detection point (CDP) (Fig. 1C). The emission is then transmitted back through the fiber to the photomultiplier tube (PMT) resulting in a sharp emission spike, labeled as intact cell in the electropherogram in

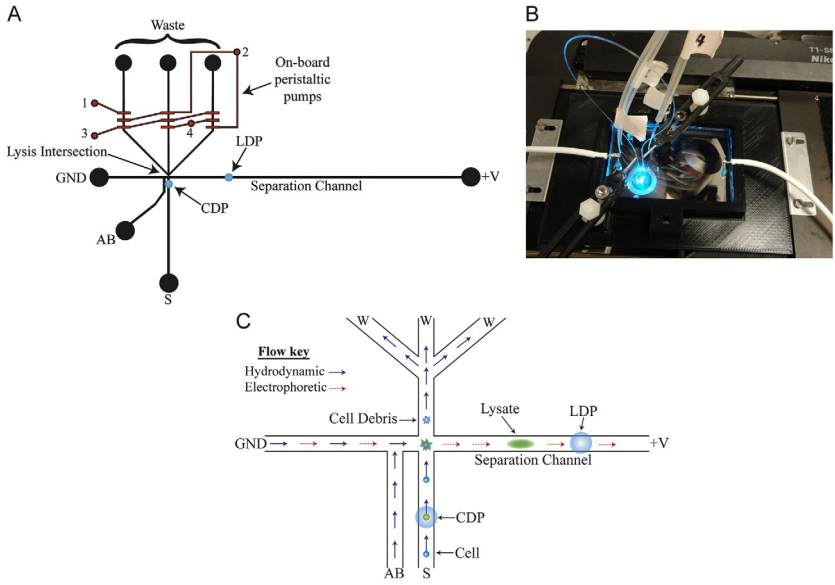


**Fig. 1** (A) Diagram of the single cell μCE-LIF device. The electric field was applied by placing the positive and ground electrodes in the reservoirs labeled "+V" and "GND", respectively. Cells are loaded into the sample reservoir, labeled "S" in the diagram. The auxiliary buffer reservoir (AB) is filled with the run buffer. Fluorescence detection of the intact cells and the lysate occurs at the cell detection point (CDP) and the lysate detection point (LDP) respectively. (B) Photograph of the device setup in the custom 3D printed microscope stage plate with the compressed air connections, HV wires and aligned optical fiber. (C) Diagram illustrating the working principles of the device.

Fig. 2A. Upon entry into the lysis intersection, the cells experience a high electric field (800–1100 V/cm). This electric field rips the cell membrane away from the charged intracellular contents, lysing the cell. As lysis occurs, the cell membrane and other debris continue with the hydrodynamic flow toward the pumps and waste reservoirs (labeled "W"). Simultaneously, the charged analytes are automatically injected toward the oppositely charged

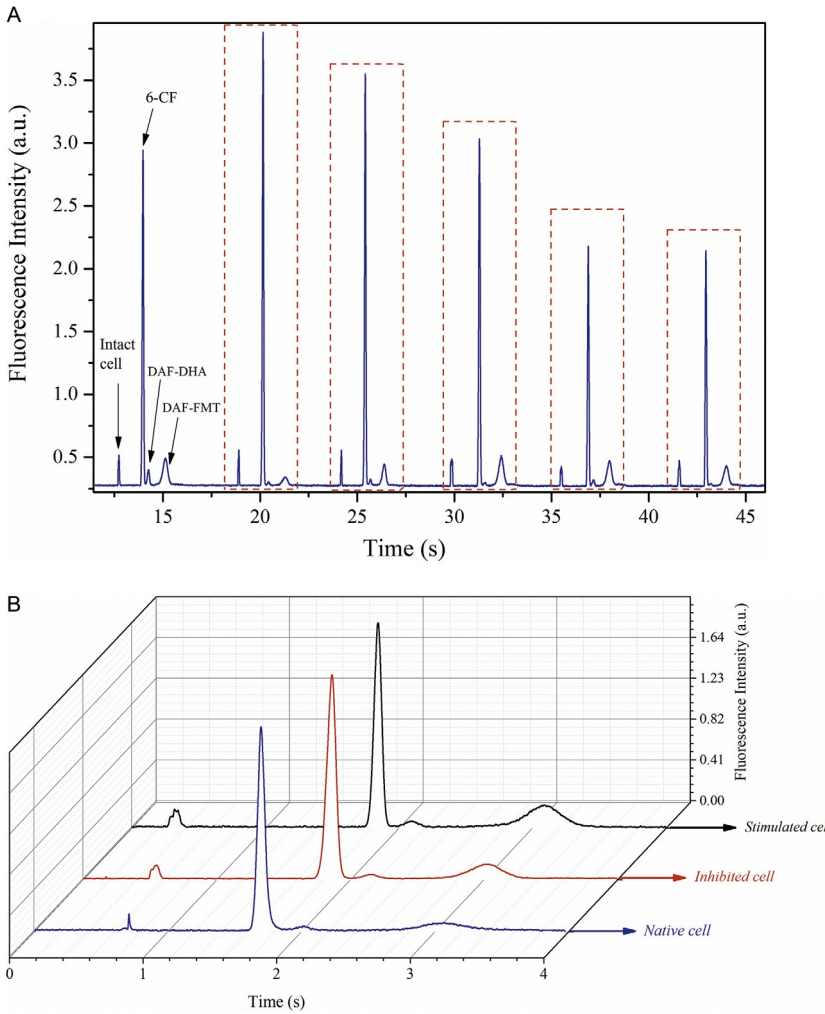


**Fig. 2** (A) An example electropherogram with intact and lysate peaks indicated for the first cell. Dotted outlines indicate single-cell electropherograms. (B) Example single-cell electropherograms for native, inhibited and stimulated conditions.

electrode (in the diagram example it is the anode) and the downstream lysate detection point (LDP) resulting in emission spikes from separated fluorescent analytes (shown in Fig. 2A).

Our device has a few key features that set it apart from other microfluidic SCA systems. The integrated peristaltic pumps allow for simple and precise control of flow rate within our device. Our pumping manifold consists of three parallel pumping channels. Each pumping channel is a three-valve peristaltic pump modeled after designs reported by the Quake group (Unger, Chou, Thorsen, Scherer, & Quake, 2000). Individual pumping units consist of three Quake-style valves in series along a fluidic channel. Flow is generated by actuating each of the valves 120° out of phase with each other generating net fluid movement in one direction. A single-channel pump can generate flow rates up to 3 nL/s, but the flow is pulsatile. By integrating three pumping channels actuated 120° out of phase with each other, our device can generate smooth flow at rates up to 9.2 nL/s. The rate at which the cells flow into the injection intersection may be controlled by adjusting the actuation pressure of the valves using a regulator. Details regarding the assembly and working principles of the on-board peristaltic pumps and the peripheral pneumatics were described in depth previously (Patabadige, Mickleburgh, et al., 2016). Additionally, the integration of the optical fiber enables fluorescence detection at two locations simultaneously without the addition of a second objective, detector, or additional optics. Placing the second detection spot prior to the injection intersection results in a signal just before cell lysis. By measuring the time between the intact cell signal and lysate signal the absolute migration time of separated species may be determined. This capability is important when multiple analyte signals must be identified and quantified.

## 3.2 Improvements in optical fiber detection

There have been several improvements made to our system with regards to the optical fiber detection since our previous publications (Patabadige, Sadeghi, et al., 2016; Sadeghi et al., 2016). Ideally, optical signals coupled between fiber optic components are transmitted with no loss of light. However, there is always some type of imperfection present at fiber optic connections that causes some loss of light. As shown in our previous reports, the theoretical coupling efficiency of optical fiber bridge, was calculated to be ~94%, but the experimental coupling efficiency for the fiber was determined to be 45 ± 5% (Sadeghi et al., 2016). There are several reasons for this

much difference including: the attenuation of multimode fiber (MMF) modes due to the bending of the optical fiber, "Fresnel reflection" at the substrate-to-air boundary, reflections at the fiber-gap-PDMS (poly(dimethyl siloxane)) boundaries, and also some refractions that have been ignored theoretically. When the MMF is aligned, optical power may be reflected back into the objective from the air-substrate, substrate-PDMS, or fiber-gap-PDMS boundaries. Light that is reflected back into the objective is considered lost. This reflection loss, called Fresnel reflection, occurs at every interface. Fresnel reflection is caused by a step change in the refractive index that here occurs at the fiber joint. In most of fiber alignments, this step change in refractive index is caused by the ends of fibers being separated by a small gap of air. Fresnel refraction occurs twice at both ends of the MMF in our optical fiber bridge design.

To reduce the amount of loss from Fresnel reflection, the air gap can be filled with a refractive index matching gel (RI gel). The refractive index of the RI gel should match the refractive index of the fiber core. RI gel reduces the step change in the refractive index at the fiber cross section, reducing Fresnel reflection. In our system, RI gel (Thorlabs G608N3) was used to reduce or eliminate Fresnel reflection. RI gels should remain transparent over time, if not, then the optical connection's loss will increase over time.

Additionally, to improve the ease-of-use of our optical fiber bridge, we employed 3D printing to design a chip holder and fiber optic alignment tools (depicted in Fig. 1B) to allow users to more easily adjust and secure the alignment of the ends of the fiber (3D drawing files are available upon request). Also, the plastic nozzles used to couple the fibers to the device in our previous publications (Patabadige, Jia, et al., 2016; Sadeghi et al., 2016) were replaced with in-house made metal fiber adapters (MFAs). These MFAs were fashioned from the barrels of 23-gauge hypodermic needles. The MFAs are not only straighter but also capable of holding the fiber firmly perpendicular to the chip channel and are also more durable compared to the plastic nozzles.

## 4. Materials and methods

### 4.1 Reagents and materials

T-lymphocyte cells (Jurkat, Clone E6–1, ATCC TIB-152), RPMI-1640 medium (ATCC 30–2001) and Dulbecco's phosphate buffered saline (D-PBS, 1 ×, ATCC 30-2200) were purchased from American Type Culture Collection (Manassas, VA). Sodium borate, lyophilized bovine serum

albumin (BSA), Tween-20, Xylenes (Certified ACS), and acetonitrile (HPLC grade) were all obtained from Fisher Scientific (Pittsburgh, PA). Sodium dodecyl sulfate, anhydrous dimethyl sulfoxide, 99.9% (DMSO), and lipopolysaccharides (LPS) from *Escherichia coli* line 0111:B4 were purchased from SigmaAldrich (St. Louis, MO). 4-Amino-5-methylamino-2′,7′-difluorofluorescein diacetate (DAF-FM DA) was purchased from Invitrogen, (Waltham, MA), in 50 μg packs. 6-Carboxyfluorescein diacetate, single isomer (6-CFDA) and probenecid sodium salt were purchased from Biotium Inc. (Fremont, CA). The iNOS inhibitor, 1400W dihydrochloride, was purchased from Tocris (Minneapolis, MN). Negative tone photoresist SU-8 2010 was purchased from MicroChem Corp. (Newton, MA). The SU-8 developer, 2-(1-methoxy) propyl acetate (99%), was obtained from Acros (Morris Plains, NJ). AZ P4620 positive tone photoresist and AZ 400K developer (1:4) were obtained from AZ Electronic Materials (Branchburg, NJ). Silicon wafers (100 mm diameter, single-side polished, mechanical grade or better) were purchased from Silicon, Inc. (Boise, ID). Chrome coated silicon wafers (100 mm diameter, single-side polished, test grade) were purchased from WRS Materials (San Jose, CA). (1,1,1,3,3,3-hexamethyldisilazane (98%) (HMDS) was purchased from Gelest (Morrisville, PA). Sylgard 184 PDMS prepolymer and curing agent were purchased from Dow Corning (Corning Inc., Corning, NY). Ultrapure water was generated from a Barnstead E-pure system (Dubuque, IA). Multimode optical fiber (0.22 NA, core Ø105 μm) was obtained from Thorlabs Inc. (Newton, NJ).

## 4.2 Device fabrication

Our device is fabricated using two layers of patterned PDMS, the bottom layer consisting of the fluidic manifold and the top containing a manifold of Quake valves (aka the pneumatic layer). The device is fabricated using standard photolithography to make silicon wafer master molds (SWMMs) for subsequent multilayer soft lithography in a manner similar to that reported previously (Patabadige, Mickleburgh, et al., 2016) detailed below.

### *4.2.1 Photolithography*

The photomasks used to generate the desired channel patters were first drawn using AutoCAD 2018 (Autodesk, San Rafael, CA) (CAD .dwg files of the designs are available upon request). The drawings were then sent to a laser photoplotting company (Fineline Imaging, Colorado Springs, CO) to be printed at a resolution of 40 kdpi. The fluidic layer pattern was printed with dark features and a clear background and the pneumatic layer pattern was printed clear with a dark background.

The fluidic SWMM was fabricated by spin coating (Laurell Technologies, North Wales, PA) positive tone photoresist AZ P4620 onto a clean, chrome coated, silicon wafer (1000 rpm for 18 s) yielding a film thickness of 18–20 μm. The coated wafer was then soft baked on a hot plate using a multistep baking process beginning with 65 °C for 2 min, followed by a quick ramp in temperature to 95 °C (approx. 30 °C/min) and held there for 2 min, and then a final quick ramp to 120 °C (approx. 30 °C/min) and held for 4 min. The baked wafer was then removed from the hotplate and placed in a laminar flow hood to cool for 20 min. The photomask with the fluidic layer features was then placed carefully onto the coated wafer and a quartz block ($4'' \times 4'' \times 0.5''$) was placed on top. The assembled wafer, photomask and quartz block were then placed in a UV flood exposure system (ThermoOriel, Stratford, CT) and exposed to UV light for the proper duration that is calculated using the prescribed UV energy dose for 20 μm film thickness (630 mJ/cm$^2$) and the measured output power of the mercury arc lamp. Following exposure, the quartz block and photomask were removed from the wafer and the wafer sat in the laminar flow hood for 10 min. The wafer was then placed into a crystallization dish filled with the AZ developer (1:4) and developed by gently swirling the developer to remove any uncured AZ. Following development, the wafer was then rinsed carefully with ultrapure water and then carefully dried using a nitrogen blowgun (<50 kPa pressure). The wafer was then placed back onto a hotplate and baked at 120 °C for 4 min and then removed from the hotplate and allowed to cool for storage until use.

The pneumatic SWMM for the upper layer of the device was fabricated using negative tone photoresist, SU-82010. The photoresist was spin coated onto a bare silicon wafer (1000 rpm for 20 s) yielding a film thickness of 20 μm. The coated wafer then underwent soft baking on the first hot plate at 65 °C for 2 min and then the second at 95 °C for 4 min. The coated wafer was then removed from the hotplate and allowed to cool for 10 min in a laminar flow hood. The photomask containing the valve manifold pattern for the upper layer was placed on top of the coated wafer followed by the quartz block and subsequently exposed for a duration calculated using the required dose for the film thickness (145 mJ/cm$^2$) and the measured output power of the mercury arc lamp. The photomask and quartz were then removed, and the wafer was then immediately hard baked (using same temperature and times as soft baking step) and allowed to cool. Then the wafer was placed into a crystallization dish containing SU-8 developer (2-(1-methoxy) propyl acetate) and developed by gently swirling the developer to remove any uncured polymer. Complete development was verified by removing the

wafer from the developer and carefully squirting a small amount of isopropanol onto the pattern. Development was complete when no white streaks appeared upon contact with isopropanol. The wafer was then carefully dried using the nitrogen blowgun as described before.

### 4.2.2 Soft lithography

Aliquots with different ratios of PDMS elastomer base to curing agent were measured into three disposable plastic cups. The masses and ratios of elastomer base and curing agent can be found in Table 1. Each of the three aliquots were separately mixed thoroughly using a coffee stirrer and then degassed for 30 min in a vacuum desiccator. The fabrication of the fluidic layer began with pretreating the fluidic SWMM by spin coating 100 μL of 1:1 HMDS:Xylenes (2000 rpm for 32 s). All of the 30:1 mixture of PDMS was poured onto the pretreated fluidic SWMM and spin coated at 2000 rpm for 32 s to generate a thin layer (50 μm thick). The coated fluidic SWMM was then placed in a curing oven (80 °C for 90 min). The valve/fiber optic layer was fabricated by pretreating the pneumatic SWMM with HMDS:Xylenes in the same manner as the fluidic SWMM. A Plexiglas frame (shown in Fig. 3A) was then aligned and placed atop the wafer according to the pattern. All of the 5:1 mixture of PDMS was poured into the frame ensuring that the entire area of the wafer within the frame is covered. The wafer was then placed in the curing oven for an initial period of 15 min. The frame was then filled to the top using a portion of the 10:1 PDMS mixture and was cured for an additional 75 min. (Note: both wafers should be curing at the same time). Both wafers were then removed and placed in a laminar flow hood to cool for 10 min. The Plexiglas frame was carefully removed from the cured valve/fiber optic layer using a scalpel. The valve/fiber optic layer was then carefully peeled off the pneumatic SWMM and the edges were trimmed of any extra PDMS skirt. With the valve/fiber optic layer face up, a custom-made Plexiglas jig (see *note* 1)

**Table 1** Ratios and amounts of elastomer base and curing agent required for the fabrication of the SCA device.

| Elastomer base:curing agent | Mass of elastomer base (g) | Mass of curing agent (g) |
|---|---|---|
| 30:1 | 6 | 0.2 |
| 5:1 | 6 | 1.2 |
| 12:1 | 24 | 2 |

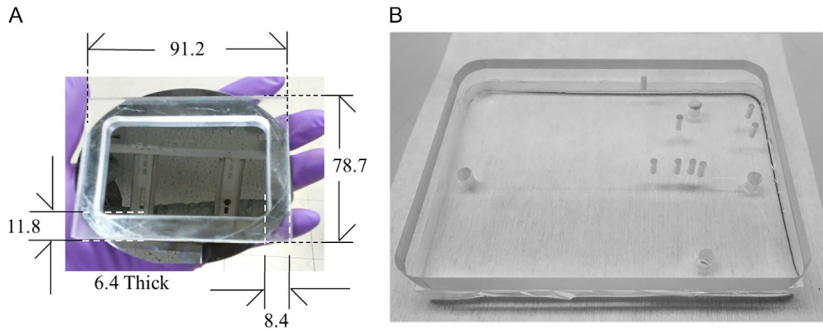


**Fig. 3** (A) Photograph of the aligned Plexiglas frame with dimensions (in mm). (B) Placement of the Plexiglas jig on top of the valve/fiber optic layer. The four holes in the upper right-hand corner were aligned with the location of the compressed air inlets on the pattern.

was placed on top of the valve/fiber optic layer, using the location of the 4 compressed air inlet holes to align the jig properly (shown in Fig. 3B) (dimensions available upon request). All holes in the valve/fiber optic layer were punched using a modified hypodermic needle (see *note* 2). Between each hole punching, the needle was cleared of any debris using a blowgun.

The valve/fiber optic layer was then peeled away from the Plexiglas jig and the patterned side was cleaned with Scotch Magic Tape (3M, Maplewood, MN) (see *note* 3). The valve/fiber optic layer was then carefully aligned and placed on top of the fluidic layer such that the fiber optic access holes were aligned with the proper features on the fluidic layer (i.e., the intact cell detection access hole aligned with the sample channel below the lysis intersection and the detection spots aligned along the separation channel) (see *note* 4).

The remaining 10:1 PDMS mixture was poured around the edges of the chip completely covering any exposed wafer and the assembled layers were then placed back in the curing oven for an additional 90 min. The assembled layers and wafer were then removed from the curing oven and allowed to cool for 10 min in a laminar flow hood. The chip was then carefully peeled off the wafer and placed patterned-side up in the laminar flow hood. The fluidic reservoirs were then punched using a 3 mm biopsy punch (Fisher Scientific, Pittsburg, PA). Finally, the PDMS skirt was trimmed off the edges such that the chip was approximately $72 \times 48$ mm.

## 4.3 Experimental setup

### 4.3.1 Preparation of electrophoresis buffer

The composition of the electrophoresis buffer was similar to that reported previously.(Patabadige, Mickleburgh, et al., 2016) The buffer consisted of 0.2% Tween20, 20% (v/v) Acetonitrile, 20 mg/mL BSA, 2 mM SDS and 25 mM sodium borate.

### 4.3.2 Preparation, setup and operation of the microfluidic device

The underside of the microfluidic device (where the fluidic channels are located) was gently but thoroughly rinsed with ultrapure water for 20–30 s. The device was then dried using a nitrogen blowgun ($P < 50$ kPa) and placed channel side up into a laminar flow hood. Any remaining debris was removed by carefully allowing a length of Scotch Magic Tape to adhere to the channel side of the device and then it was carefully peeled away. Both sides of a microscope slide ($75 \times 50 \times 1.0$ mm) (Fisher Scientific, Pittsburg, PA) were cleaned using glassware soap and thoroughly scrubbed with a cleanroom swab (TX714MD, Texwipe, Kernersville, NC). The slide was then thoroughly rinsed for 20–30 s with ultrapure water and dried using a nitrogen blowgun. In the laminar flow hood, the microfluidic device was assembled by carefully layering the device atop the cleaned glass slide and carefully removing any air bubbles by gently pressing on the top of the device using a gloved hand. Any dust or debris on the top of the device was then removed using Scotch Magic Tape to ensure minimal light scattering.

The device was then placed into the 3D printed chip holder and secured into the 3D printed microscope stage plate and placed in the xy translation stage of the microscope. The channels were allowed to fill passively by filling the reservoir (labeled "GND" in Fig. 1A) with 30 μL of prewarmed electrophoresis buffer (37 °C). Once all fluidic channels were filled with electrophoresis buffer, all reservoirs were filled with 30 μL of electrophoresis buffer (see *note* 5).

Once the device was filled, the HV wires (39x2215,22 AWG, Allied Electronics inc., Fort Worth, TX) with a short length of platinum wire (approx. 2 cm) soldered to one end were press fit into the wire slots on the chip holder with the platinum wire in the "GND" and "+V" reservoirs (Fig. 1A). The HV wire in the "GND" reservoir was connected to ground and the "+V" reservoir was connected to the output of the HV power supply (Spellman CZE1000R, Spellman High Voltage Electronics, Hauppauge, NY).

The on-board peristaltic pumps were actuated using four mounted solenoid valves (LHDA1221111H, The Lee Company, Westbrook, CT) mounted on a manifold (LFMX0510538BE, The Lee Company, Westbrook, CT) connected to a compressed air regulator (Norgren inc., Littleton, CO) which was connected to the building compressed air (120 psi) and regulated to deliver pressures between 0 and 2 bar. The actuation pattern of the solenoid valves was controlled by a microcontroller (pro trinket 5 V, Adafruit, New York City, NY) programmed with in-house written code (available upon request). The voltage of the digital control signals from the microcontroller (5 V) was stepped up to the actuation voltage of the solenoids (12 V) using the L298N H-bridge (Elegoo inc., Shenzhen, China). A full wiring diagram for the pneumatic controls is available upon request. The compressed air outlets of the manifold were then connected to the appropriate inlets on the device, labeled 1–4 in Fig. 1A.

#### 4.3.3 Preparation and setup of the optical fiber and LIF detection

The MFAs were prepared by applying a small amount of RI gel to one end and inserting that end into their respective fiber optic access holes. Both ends of the MMF (105/125 μm core/cladding, Thorlabs FG105UCA, N.A. = 0.22) were then prepared by stripping the coating material near the ends and cleaning the fiber surfaces with an optical wiping tissue wet with isopropanol. The fiber ends were then cleaved using a mechanical fiber cleaver (FC-6S, Sumitomo Electric Lightwave Corp., Raleigh, NC) and inserted into the prepared MFAs. The fiber was bridged between the CDP in the cell handling channel and the LDP in the separation channel (Fig. 1C).

The excitation source was a 488 nm laser diode (Oxxius-LBX-488-100-CSB-PP). As illustrated in our previous publication (Sadeghi et al., 2016), several optical elements (i.e., elliptical mirrors and an iris diaphragm) were used to direct the beam into the rear port of a commercial inverted Nikon TS-100-F microscope (Nikon Instruments, Inc., Melville, NY) equipped with a fluorescence filter cube (XF115–2 FITC, Omega Optical, Brattleboro, VT). A 20× microscope objective (NA = 0.45) and *Z*-axis control (i.e., focusing knob) were used to control the spot size of a laser beam. The fluorescence signal was detected by a PMT (R-928, Hamamatsu Instruments, Bridgewater, NJ) with an 800 μm diameter pinhole.

#### 4.3.4 Data collection and analysis

The signal current from the PMT was amplified (5 μA/V) and filtered (30 Hz, low-pass) using a low-noise current preamplifier (Stanford

Research Systems, Sunnyvale, CA). Data were collected using a differential analog input of a USB data acquisition device (USB-6002) and a program written in-house using LabVIEW (National Instruments, Austin, TX). Data visualization and analysis was performed using IgorPro (WaveMetrics, Portland, OR).

## 4.4 Cell culture and preparation

### 4.4.1 Cell culture

Cells were cultured in RPMI 1640 medium containing 10% (v/v) fetal bovine serum, L-glutamine (2 mM), penicillin (100 μg/mL), and streptomycin (100 μg/mL). The cells were maintained in a humidified environment at 37 °C and 5% $CO_2$ and cultured in 25 mL polystyrene culture flasks (Corning Cell Culture Treated, Fisher Scientific). Cells were passaged every 2–3 days. All experiments were scheduled to ensure that the cell density would be approximately $10^6$ cells/mL immediately prior to labeling.

### 4.4.2 LPS stimulation and iNOS inhibition

LPS stimulation of NO production in cells was performed in a manner similar to that reported previously (Metto et al., 2013). Briefly, cells were stimulated using purified lipopolysaccharide (LPS). LPS was added at a rate of 3 μL of 1 mg/mL LPS per milliliter of cell suspension of healthy Jurkat cells and placed back in the incubator for a period of 3 h. For inhibition experiments, the cells were treated with the same concentration of LPS with the addition of iNOS inhibitor, 1400W HCl, with a final concentration of 100 μM.

### 4.4.3 Preparation and analysis of cells

Native, stimulated, and inhibited cells were labeled using the same procedure and similar to that reported previously (Metto et al., 2013). A stock solution of the fluorogenic NO probe, DAF-FM DA, (approx. 1 mM) was prepared by dissolving the contents of single pack in 100 μL of DMSO. A separate stock solution of internal standard, 6-CFDA (3.74 mM), was also prepared using DMSO. To prevent the efflux of the anionic dyes probenecid, a commonly used inhibitor of MRP1 (Di Virgilio, Steinberg, & Silverstein, 1990), was used. Stock solution of probenecid was prepared by dissolving 77 mg in 1 mL of PBS (250 mM). An amount of 1 mL of cell suspension was aliquoted into a 1.5 mL Eppendorf tube and then centrifuged at 125 × *g* (Marathon 8 K, Fisher Scientific, Pittsburgh, PA) for 5 min. The

supernatant was removed from the pellet and discarded. Cells were resuspended in a mixture containing 1.1 μL of 6-CFDA stock solution, 15 μL of DAF-FM DA stock solution, 1 μL of probenecid stock solution and 82.9 μL sterile PBS (100 μL total) and incubated for 30 min at 37 °C on a heat block. The labeled cells were then diluted to 1 mL with sterile PBS prewarmed to 37 °C and centrifuged at 125 × *g* for 5 min, and the supernatant was then discarded. These rinsing steps were repeated twice more with 1 mL portions of sterile PBS followed by a final resuspension in 1 mL of sterile PBS containing 2 mg/mL BSA and 2.5 mM probenecid.

An amount of 30 μL of labeled cell suspension was then loaded into the sample reservoir (labeled "S" in Fig. 1A) on the microfluidic device for analysis, while the remaining cell suspension remained on the heat block (Fisher Scientific, Pittsburg PA) at 37 °C until more cell suspension was needed. Operation of the device began by turning on the on-board peristaltic pumps and setting the actuation pressure to result in a modest flow rate (<1 bar). Verification of cell movement and sufficient fluorescence labeling was done visually. The electric field was then applied to the separation channel (850 V/cm). Adjustments to the actuation pressure were made by observing cell lysis at the intersection and determining whether the cells are moving too fast (i.e., a large portion of intracellular fluorescence continues on to the waste channel) or too slow (i.e., the entirety of the cell contents along with the membrane are injected down the separation channel). Typical flow rates for efficient lysis in our system fall in the range of 2–4 nL/s (see *note* 6). Once the conditions for lysis have been optimized the objective was then directed toward the downstream end of the optical fiber at the LDP and the optical path was switched from the eyepiece to the PMT (see *note* 7). Successful alignment of the fiber and optimal lysis will result in an electropherogram resembling that shown in Fig. 2A.

Changes in intracellular NO levels were quantified for native, stimulated, and inhibited cells. These changes were measured by computing the ratio of the fluorescence peak areas of DAF-FM T to those of 6-CF for each cell. An overlay of representative single-cell electropherograms from each of the 3 runs is shown in Fig. 2B. A summary of the results from the experiments is shown in Table 2. It is also important to mention that better quantitation of NO in this study was achieved due to the absence of an extra internal standard peak that was present in our previous publication (Metto et al., 2013). We believe that this was a result of using an internal standard from a different vendor, i.e., a different lot.

**Table 2** The average ratios (DAF FM T/6-CF ± standard deviation) of peak area and peak height for native, stimulated and inhibited cells.

| Peak area ratio | DAF FM T/6-CF | No. of cells |
|---|---|---|
| Native cells | 0.31 ± 0.15 | 53 |
| Stimulated cells | 0.68 ± 0.29 | 44 |
| Inhibited | 0.37 ± 0.17 | 66 |
| Peak height ratio | DAF FM T/6-CF | No. of cells |
| Native cells | 0.067 ± 0.031 | 53 |
| Stimulated cells | 0.18 ± 0.08 | 44 |
| Inhibited | 0.11 ± 0.05 | 66 |

## 5. Notes

1. The jig was made using ¼″ thick acrylic (Plexiglas) that was cut to the specified shape and size. Holes were then drilled at the precise locations using a manual vertical mill with a number 54 drill bit (0.0550″ O.D.) to serve as guides for the hole punching locations for the compressed air inlets and the fiber optic access holes.
2. The bevel of a 1 ½″, 18-gauge hypodermic needle was sawed off using a rotary tool with a heavy-duty cut-off wheel (Dremel, Mount Prospect, IL). The sawed-off edge was then deburred using a fine-tip cone high speed cutter bit and sharpened using 400 grit sand paper.
3. Scotch tape is used to clean the device of particulate and debris both during the fabrication process as well as pre and post analysis. Cleaning is done by tearing off and discarding the length of tape between the roll and the blade as this may have been exposed to dust particles if stored in the open. Then a 3–4″ inch long piece of tape is torn off being careful to not allow it to touch any surface. Then the length of tape is draped across the surface and then peeled up repeatedly until the entire surface has been cleaned.
4. Alignment may be facilitated by using a binocular magnifying headband with 5 × lenses (Optivisor, Donegan Optical Company Inc., Lenexa, KS).
5. Any bubbles in the channels may be removed by emptying the reservoir located closest to the bubble and applying suction to the reservoir until the bubble is cleared.

6. The optimal electric field magnitude and flow rate must be found experimentally and varies between different cell lines and buffer conductivity and composition. It is crucial that the electric field be of sufficient strength to generate cellular lysis. In general, the lower limit of field strength is determined by the resulting flow rate of the lowest actuation pressure at which reasonable cellular movement occurs. The upper limit is determined by the device's capability to dissipate power (between 5 and 10 W/m generally).
7. The focus may require adjustment to obtain optimal signal when switching between the eyepiece and the detector as the optical pathlength may differ.

## 6. Conclusion

Herein we have fully described the design, fabrication and operation of our μCE-LIF system for the analysis of single cells. As a demonstration of the utility of our system, we applied it to the analysis of intracellular NO in T-lymphocytes under native, LPS stimulated, and inhibited conditions. As expected, we observed a marked increase in NO levels upon stimulation with LPS in comparison with the native cells and a decrease in NO with the addition of the iNOS inhibitor 1400W dihydrochloride. It is important to note that this is the first time we are reporting the use of our device to measure the effects on an inhibitor on the production of intracellular NO. This demonstrates the potential applicability of our system for the study of the effects of novel pharmaceutical agents for the treatment of diseases associated with inflammation, such as Alzheimer's, Parkinson's, cardiovascular disease, and cancers (Pacher et al., 2007).

The system presented in this chapter is the result of many years of work done by several researchers. We believe that we have reached the point where our system is robust enough to be used for the analysis of a variety of enzyme activities at the single cell level. It is our hope that the information in this chapter may help other research groups to directly use, or adapt for their purposes, our single-cell analysis device.

## Acknowledgments

This research was funded by NSF Grants CHE-1411993, CBET-1159966 and CBET-1337438. J.S. and J.S. were supported by the Johnson Cancer Center, Kansas State University.

## References


Bektik, E., Dennis, A., Prasanna, P., Madabhushi, A., & Fu, J. D. (2017). Single cell qPCR reveals that additional HAND2 and microRNA-1 facilitate the early reprogramming progress of seven-factor-induced human myocytes. *PLoS One*, *12*(8), e0183000. https://doi.org/10.1371/journal. pone.0183000.

Bogdan, C. (2001). Nitric oxide and the immune response. *Nature Immunology*, *2*(10), 907–916. https://doi.org/10.1038/ni1001-907.

Caruso, G., Fresta, C. G., Siegel, J. M., Wijesinghe, M. B., & Lunte, S. M. (2017). Microchip electrophoresis with laser-induced fluorescence detection for the determination of the ratio of nitric oxide to superoxide production in macrophages during inflammation. *Analytical and Bioanalytical Chemistry*, *409*(19), 4529–4538. https://doi.org/10.1007/s00216-017-0401-z.

Chen, Z., Li, Q., Sun, Q., Chen, H., Wang, X., Li, N., et al. (2012). Simultaneous determination of reactive oxygen and nitrogen species in mitochondrial compartments of apoptotic HepG2 cells and PC12 cells based on microchip electrophoresis-laser-induced fluorescence. *Analytical Chemistry*, *84*(11), 4687–4694. https://doi.org/10.1021/ac300255n.

Di Virgilio, F., Steinberg, T. H., & Silverstein, S. C. (1990). Inhibition of Fura-2 sequestration and secretion with organic anion transport blockers. *Cell Calcium*, *11*(2–3), 57–62.

Dickinson, A. J., Meyer, M., Pawlak, E. A., Gomez, S., Jaspers, I., & Allbritton, N. L. (2015). Analysis of sphingosine kinase activity in single natural killer cells from peripheral blood. *Integrative Biology: Quantitative Biosciences From Nano to Macro*, 7(4), 392–401. https://doi.org/10.1039/c5ib00007f.

Mainz, E. R., Gunasekara, D. B., Caruso, G., Jensen, D. T., Hulvey, M. K., da Silva, J. A. F., et al. (2012). Monitoring intracellular nitric oxide production using microchip electrophoresis and laser-induced fluorescence detection. *Analytical Methods*, *4*(2), 414–420. https://doi.org/10.1039/c2ay05542b.

Metto, E. C., Evans, K., Barney, P., Culbertson, A. H., Gunasekara, D. B., Caruso, G., et al. (2013). An integrated microfluidic device for monitoring changes in nitric oxide production in single T-lymphocyte (Jurkat) cells. *Analytical Chemistry*, *85*(21), 10188–10195. https://doi.org/10.1021/ac401665u.

Pacher, P., Beckman, J. S., & Liaudet, L. (2007). Nitric oxide and peroxynitrite in health and disease. *Physiological Reviews*, *87*(1), 315–424. https://doi.org/10.1152/physrev.00029.2006.

Patabadige, D. E., Jia, S., Sibbitts, J., Sadeghi, J., Sellens, K., & Culbertson, C. T. (2016). Micro total analysis systems: Fundamental advances and applications. *Analytical Chemistry*, *88*(1), 320–338. https://doi.org/10.1021/acs.analchem.5b04310.

Patabadige, D. E., Mickleburgh, T., Ferris, L., Brummer, G., Culbertson, A. H., & Culbertson, C. T. (2016). High-throughput microfluidic device for single cell analysis using multiple integrated soft lithographic pumps. *Electrophoresis*, *37*(10), 1337–1344. https://doi.org/10.1002/elps.201500557.

Patabadige, D. E., Sadeghi, J., Kalubowilage, M., Bossmann, S. H., Culbertson, A. H., Latifi, H., et al. (2016). Integrating optical fiber bridges in microfluidic devices to create multiple excitation/detection points for single cell analysis. *Analytical Chemistry*, *88*(20), 9920–9925. https://doi.org/10.1021/acs.analchem.6b03133.

Proctor, A., Herrera-Loeza, S. G., Wang, Q., Lawrence, D. S., Yeh, J. J., & Allbritton, N. L. (2014). Measurement of protein kinase B activity in single primary human pancreatic cancer cells. *Analytical Chemistry*, *86*(9), 4573–4580. https://doi.org/10.1021/ac500616q.

Sadeghi, J., Patabadige, D. E., Culbertson, A. H., Latifi, H., & Culbertson, C. T. (2016). Out-of-plane integration of a multimode optical fiber for single particle/cell detection at multiple points on a microfluidic device with applications to particle/cell counting, velocimetry, size discrimination and the analysis of single cell lysate injections. *Lab on a Chip*, *17*(1), 145–155. https://doi.org/10.1039/c6lc01161f.

Sibbitts, J., Sellens, K. A., Jia, S., Klasner, S. A., & Culbertson, C. T. (2018). Cellular analysis using microfluidics. *Analytical Chemistry*, *90*(1), 65–85. https://doi.org/10.1021/acs.analchem.7b04519.

Turner, A. H., Lebhar, M. S., Proctor, A., Wang, Q., Lawrence, D. S., & Allbritton, N. L. (2016). Rational design of a dephosphorylation-resistant reporter enables single-cell measurement of tyrosine kinase activity. *ACS Chemical Biology*, *11*(2), 355–362. https://doi.org/10.1021/acschembio.5b00667.

Unger, M. A., Chou, H. P., Thorsen, T., Scherer, A., & Quake, S. R. (2000). Monolithic microfabricated valves and pumps by multilayer soft lithography. *Science*, *288*(5463), 113–116.

Wang, Y., Li, J., Feng, L., Yu, J., Zhang, Y., Ye, D., et al. (2016). Lysosome-targeting fluorogenic probe for Cathepsin B imaging in living cells. *Analytical Chemistry*, *88*(24), 12403–12410. https://doi.org/10.1021/acs.analchem.6b03717.